

Supporting information

Homochiral Metal Phosphonate Nanotubes**

Xun-Gao Liu, Song-Song Bao, Jian Huang, Kazuya Otsubo, Jian-Shen Feng, Min Ren, Feng-Chun Hu, Zhihu Sun, Yi-Zhi Li, Li-Min Zheng,* Shiqiang Wei,* Hiroshi Kitagawa*

Experimental Section

Materials and measurements. (*S*)- and (*R*)-1-phenylethylamine were purchased from Aldrich without further purification, and all the other starting materials were of reagent grade quality. (*S*)-, (*R*)-(1-phenylethylamino)methylphosphonic acid (pempH₂) were prepared by reactions of (*S*)- or (*R*)-1-phenylethylamine, diethyl phosphite and paraformaldehyde, according to the literature method.¹ The elemental analyses were performed in a PE240C elemental analyzer. The infrared spectra were recorded on a VECTOR 22 spectrometer with pressed KBr pellets. The powder XRD patterns were recorded on a Bruker D8 ADVANCE X-ray diffractometer. CD spectra were measured on a JASCO J-720W spectrophotometer at room temperature. Approximate estimations of the second-order-nonlinear optical intensity were obtained by comparison of the results obtained from a powder sample (80±150 mm diameter) in the form of a pellet (Kurtz powder test²), with that obtained for urea. A pulsed Q-switched Nd:YAG laser at a wavelength of 1064 nm was used to generate the SHG signal. The backward-scattered SHG light was collected using a spherical concave mirror and passed through a filter that transmits only 532 nm radiation. Thermal analyses were performed in nitrogen in the temperature range 25 – 650 °C with a heating rate of 10 °C min⁻¹ on a TGA-DTA V1.1b Inst 2100 instrument. The solvent absorption and desorption isotherms were conducted by a BELSORP-Max adsorption analyzer. The N₂ adsorption isotherms were performed by a Micromeritics ASAP 2020M volumetric adsorption analyzer.

Syntheses. Compounds *R*-1, *S*-1, *R*-2 and *S*-2 were synthesized under similar experimental conditions except the pH (~ 5.6 for **1** and ~ 6.1 for **2**). A typical procedure for the preparation of *R*-1 is described as below. A mixture of CoSO₄·7H₂O (0.1 mmol, 0.0281), and *R*-pempH₂ (0.1 mmol, 0.0255 g) in 10 mL of H₂O, adjusted to pH 5.6 with 1 M NaOH, was kept in a Teflon-lined autoclave at 140 °C for 4 days. After cooling to room temperature, purple needle-like crystals of compound *R*-1 were obtained. Yield: 53%. Elemental analysis calcd (%) for C₉H₁₆CoNO₅P: C, 35.08; H, 5.23; N, 4.55%; found: C, 35.07; H, 5.22; N, 4.49%. IR (KBr, cm⁻¹): 3554 (w), 3277(m), 3103(w), 2917(w), 1618(w), 1495(w), 1453(w), 1281(w), 1195(w), 1109(m), 1083(s), 983 (s), 950(w), 894(w), 849(w), 768(m), 705(m), 578(w), 551(m), 489(m).

For *S-1*: Yield: 51%. Elemental analysis calcd (%) for $C_9H_{16}CoNO_5P$: C, 35.08; H, 5.23; N, 4.55%. Found: C, 34.89; H, 5.27; N, 4.48%. IR (KBr, cm^{-1}): 3565 (m), 3277(s), 3102(s), 2917(w), 1601(w), 1495(w), 1454(m), 1281(w), 1195(w), 1109(m), 1082(s), 983 (s), 949(w), 894(w), 847(w), 768(m), 705(m), 578(w), 550(m), 488(m).

For *R-2*: Green needle-like crystals were obtained. Yield: 48%. Elemental analysis calcd (%) for $C_9H_{16}NiNO_5P$: C, 35.11; H, 5.24; N, 4.55%. Found.: C, 35.01; H, 5.21; N, 4.41%. IR (KBr, cm^{-1}): 3518 (w), 3277(w), 3062(m), 2925(w), 1618(w), 1495(w), 1437(w), 1282(w), 1193(w), 1109(m), 1085(s), 982 (s), 929(w), 897(w), 854(w), 769(m), 706(m), 582(w), 552(w), 493(m).

For *S-2*: Yield: 51%. Elemental analysis calcd (%) for $C_9H_{16}NiNO_5P$: C, 35.11; H, 5.24; N, 4.55%. Found: C, 34.97; H, 5.21; N, 4.39%. IR (KBr, cm^{-1}): 3527 (w), 3277(w), 3061(m), 2925(w), 1602(w), 1495(w), 1454(w), 1282(w), 1193(w), 1109(m), 1084(s), 982(s), 928(w), 897(w), 853(w), 768(m), 705(m), 582(w), 552(w), 493(m).

Crystallographic studies. Data collections for complexes *R-1*, *S-1* and *S-2* were carried out on a Saturn 70 CCD diffractometer. Hemisphere of data were collected in the θ range of 2.22–26.00 for *R-1*, 2.23–26.00 for *S-1*, 2.25–27.48 for *S-2*. The data were integrated using the Siemens SAINT program,³ with the intensities corrected for Lorentz factor, polarization, air absorption, and absorption due to variation in the path length through the detector faceplate. Empirical absorption and extinction corrections were applied. The structures were solved by direct method and refined on F^2 by full-matrix least squares using SHELXTL.⁴ All the non-hydrogen atoms were refined anisotropically. All the hydrogen atoms except those attached to water molecules were put in calculated positions and refined isotropically with the isotropic vibration parameters related to the non-hydrogen atoms to which they are bonded. The hydrogen atoms attached to water molecules were found from Fourier maps and were refined isotropically. CCDC 696828 - 696830 contains the supplementary crystallographic data for this paper. These data can be obtained free of charge from the Cambridge Crystallographic Data Centre via www.ccdc.cam.ac.uk/data_request/cif.

EXAFS measurements and data analyses. The EXAFS measurements at the Ni-K edge (8333 eV) and Co-K edge (7709 eV) were carried out in transmission mode at the beamline U7C in the National Synchrotron Radiation Laboratory (NSRL) in China. The storage ring of NSRL was run at 0.8 MeV with the maximum current of 250 mA. A double crystal Si(111) monochromator was used. The nickel and cobalt foils standard were purchased from the commercial source. In a typical experiment, about 45 mg of sample was ground into fine powder and mixed with ca. 116 mg of BN and then pressed into a 13.0 mm diameter circular sample holder. The spectrum of nickel foil was recorded periodically to check the energy calibration, and the first derivative of the nickel foil K-edge spectrum at 8333 eV and the cobalt foil K-edge

spectrum at 7709 eV were used to define the zero-energy reference point. The XANES spectra were background subtracted and were normalized to the edge step at the beginning of the EXAFS oscillations in order to make a meaningful comparison of the intensity of the pre-edge features. The EXAFS signals, $\chi(k)$, were extracted from the absorption raw data, $\mu(E)$, with ATHENA 0.8.056 program⁵ choosing the energy edge value (E_0) at the maximum derivative. The quantitative analysis was carried out with the IFEFFIT 1.2.11-ARTEMIS 0.8.012 programs⁶ with the atomic models described below. Theoretical EXAFS signals were computed with the FEFF7.0 code⁷ using muffin-tin potentials and the Hedin-Lunqvist approximation for the energy-dependent part. The free-fitting parameters used in the analysis were: S_0^2 (common amplitude parameter), ΔE_0 (the refinement of the edge position), R (the interatomic distance) and σ^2 (the Debye-Waller factor).

The structural parameters were determined by a curve-fitting procedure in R space by using the ARTEMIS program and USTCXAFS software packages. The employed fitting ranges are summarized in Tables S3 and S4. The intrinsic reduction factor S_0^2 , the edge-energy shift ΔE_0 , the coordination number N , the inter-atomic distance R and the mean-square relative displacement σ^2 were fitted. The results concerning N and R are summarized in Table S5 and S6.

References

- (1) M. I. Kabachnik, T. Y. Medved', G. K. Kozlova, V. S. Balabukha, E. A. Mironova, L. I. Tikhonova, *Izvest. Akad. Nauk SSSR, Ser. Khim.* **1960**, 651.
- (2) S. K. Kurtz, T. T. Perry, *J. Appl. Phys.* **1968**, 39, 3798.
- (3) SAINT, Program for Data Extraction and Reduction, Siemens Analytical X-ray Instruments, Madison, WI, **1994–1996**.
- (4) SHELXTL (version 5.0), Reference Manual, Siemens Industrial Automation, Analytical Instruments, Madison, WI, **1995**.
- (5) B. Ravel, M. J. Newville, *Synchrotron Radiat.* **2005**, 12, 537–541.
- (6) M. J. Newville, *Synchrotron Radiat.* **2001**, 8, 322–324.
- (7) J. M. De Leon, J. J. Rehr, S. I. Zabinsky, R. C. Albers, *Phys. Rev. B* **1991**, 44, 4146.

Table S1. Crystallographic data for compounds **R-1**, **S-1**, **R-2** and **S-2**.

| Compound | R-1 | S-1 | R-2 | S-2 |
|---|--|--|--|--|
| Formular | C ₉ H ₁₆ CoNO ₅ P | C ₉ H ₁₆ CoNO ₅ P | C ₉ H ₁₆ NiNO ₅ P | C ₉ H ₁₆ NiNO ₅ P |
| <i>M</i> | 308.13 | 308.13 | 307.91 | 307.91 |
| Crystal size (mm) | 0.20×0.03×0.03 | 0.10×0.02×0.02 | 0.50×0.02×0.01 | 0.18×0.04×0.03 |
| Crystal system | Hexagonal | Hexagonal | Hexagonal | Hexagonal |
| Space group | <i>P</i> 6 ₃ | <i>P</i> 6 ₃ | <i>P</i> 6 ₃ | <i>P</i> 6 ₃ |
| <i>a</i> (Å) | 18.314(1) | 18.288(8) | 18.1621(6) | 18.081(2) |
| <i>c</i> (Å) | 6.168(1) | 6.168(4) | 6.168(7) | 6.1296(6) |
| <i>V</i> (Å ³) | 1791.9(2) | 1786.5(1) | 1762(2) | 1735.5(3) |
| <i>Z</i> | 6 | 6 | 6 | 6 |
| <i>D</i> _c (g cm ⁻³) | 1.713 | 1.718 | 1.741 | 1.768 |
| μ (mm ⁻¹) | 1.579 | 1.584 | 1.796 | 1.824 |
| <i>F</i> (000) | 954 | 954 | 960 | 960 |
| <i>R</i> _{int} | 0.062 | 0.069 | 0.080 | 0.056 |
| GOF | 1.03 | 1.05 | 0.94 | 1.09 |
| <i>R</i> ₁ , <i>wR</i> ₂ [<i>I</i> >2σ(<i>I</i>)] ^a | 0.045, 0.141 | 0.052, 0.123 | 0.049, 0.063 | 0.031, 0.082 |
| <i>R</i> ₁ , <i>wR</i> ₂ (all data) | 0.051, 0.152 | 0.060, 0.126 | 0.094, 0.074 | 0.035, 0.103 |
| Flack parameter | 0.03(3) | 0.06(3) | 0.05(4) | 0.02(2) |
| (Δρ) _{max} , (Δρ) _{min} (eÅ ⁻³) | 0.85, -0.69 | 0.41, -0.60 | 0.66, -0.47 | 0.95, -0.52 |
| CCDC | 696828 | 696829 | 1060995 | 696830 |

Table S2. Selected bond lengths (Å) and angles (°) for compounds **R-1**, **S-1**, **R-2** and **S-2**.

| | R-1 | S-1 | R-2 | S-2 |
|------------|------------|------------|------------|------------|
| M1-O1 | 2.070(4) | 2.072(5) | 2.054(6) | 2.052(3) |
| M1-O1W | 2.180(4) | 2.166(4) | 2.094(6) | 2.099(2) |
| M1-O2W | 2.156(6) | 2.157(4) | 2.080(6) | 2.075(3) |
| M1-N1 | 2.236(5) | 2.243(6) | 2.166(8) | 2.156(3) |
| M1-O2A | 2.079(5) | 2.082(4) | 2.091(6) | 2.074(3) |
| M1-O3B | 2.100(5) | 2.091(5) | 2.089(7) | 2.086(3) |
| P1-O1 | 1.536(4) | 1.522(4) | 1.532(7) | 1.534(3) |
| P1-O2 | 1.534(5) | 1.535(4) | 1.534(7) | 1.529(3) |
| P1-O3 | 1.515(4) | 1.531(4) | 1.525(7) | 1.520(3) |
| O1-M1-O1W | 87.9(1) | 88.2(1) | 89.3(3) | 89.3(1) |
| O1-M1-O2W | 84.3(1) | 84.6(1) | 84.7(2) | 84.3(1) |
| O1-M1-N1 | 82.4(7) | 82.4(1) | 83.2(3) | 84.1(2) |
| O1-M1-O2A | 170.1(1) | 169.6(1) | 171.5(3) | 171.3(1) |
| O1-M1-O3B | 89.2(1) | 89.2(1) | 88.1(2) | 88.2(1) |
| O1W-M1-O2W | 88.9(1) | 88.6(1) | 90.5(2) | 90.1(1) |
| O1W-M1-N1 | 85.8(1) | 86.3(1) | 86.8(3) | 86.9(1) |
| O1W-M1-O2A | 86.0(1) | 85.1(1) | 87.0(3) | 87.2(1) |
| O1W-M1-O3B | 174.3(1) | 174.4(1) | 174.1(3) | 174.0(1) |
| O2W-M1-N1 | 166.0(2) | 166.2(1) | 167.6(2) | 168.0(1) |
| O2b-M1-O2W | 87.7(2) | 87.2(1) | 87.8(2) | 87.7(1) |
| O2W-M1-O3B | 95.6(1) | 96.0(1) | 94.6(2) | 95.0(1) |
| O2B-M1-N1 | 104.9(1) | 105.0(1) | 104.2(3) | 103.6(1) |
| O3C-M1-N1 | 88.9(1) | 88.4(1) | 87.6(3) | 87.3(1) |
| O2B-M1-O3B | 97.3(1) | 97.9(1) | 96.3(3) | 95.8(1) |

Symmetry codes: A: x, y, 1+z; B: 1+x-y, 1+x, 1/2+z.

Table S3. Forward Fourier Transform and backward Fourier Transform selected parameters of the Co-N/O first shell at Co-K edge of *R-1*.

| Sample | Shell | K-range | Window type | R-range | Window type |
|-------------------|--------|--------------|-------------|-------------|-------------|
| <i>R-1</i> | Co-O/N | 2.375~11.593 | hanning | 1.083~1.996 | hanning |
| <i>R-1-de</i> | Co-O/N | 2.416~11.428 | hanning | 1.050~1.978 | hanning |
| <i>R-1-re</i> | Co-O/N | 2.379~11.946 | hanning | 1.050~1.977 | hanning |
| <i>R-1-100 °C</i> | Co-O/N | 2.375~11.693 | hanning | 1.101~1.990 | hanning |
| <i>R-1-120 °C</i> | Co-O/N | 2.375~11.756 | hanning | 1.050~1.978 | hanning |
| <i>R-1-130 °C</i> | Co-O/N | 2.338~11.593 | hanning | 1.050~1.996 | hanning |
| <i>R-1-140 °C</i> | Co-O/N | 2.434~11.468 | hanning | 1.050~1.978 | hanning |
| <i>R-1-180 °C</i> | Co-O/N | 2.497~11.530 | hanning | 1.050~2.009 | hanning |

Table S4. Forward Fourier Transform and backward Fourier Transform selected parameters of the Ni-N/O first shell at Ni-K edge of *R-2*.

| Sample | Shell | K-range | Window type | R-range | Window type |
|---------------|--------|--------------|---------------|-------------|---------------|
| <i>R-2</i> | Ni-O/N | 2.362~11.780 | kaiser-bessel | 1.066~1.986 | kaiser-bessel |
| <i>R-2-de</i> | Ni-O/N | 2.362~11.780 | kaiser-bessel | 1.012~1.959 | kaiser-bessel |

Table S5. Local structural fitting parameters of the Co-O and Co-N shells around Co in *R-1*, *R-1* pre-heated at different temperatures, and rehydrated sample of *R-1*-180°C.

| Sample | Shell | R | N | S_0^2 | ΔE_0 | σ^2 | R-factor |
|-------------------|-------|------|-----|---------|--------------|------------|----------|
| <i>R-1</i> | Co-O | 2.07 | 5.0 | 1.00 | 1.13 | 0.0074 | 0.0020 |
| | Co-N | 2.25 | 1.0 | 1.00 | 1.71 | 0.0058 | |
| <i>R-1</i> -100°C | Co-O | 2.07 | 5.0 | 1.00 | 0.86 | 0.0074 | 0.0043 |
| | Co-N | 2.24 | 1.0 | 1.00 | 2.54 | 0.0059 | |
| <i>R-1</i> -120°C | Co-O | 2.07 | 5.0 | 1.00 | 0.34 | 0.0092 | 0.0064 |
| | Co-N | 2.21 | 1.0 | 1.00 | 1.54 | 0.0060 | |
| <i>R-1</i> -130°C | Co-O | 1.98 | 3.0 | 1.00 | -1.11 | 0.0065 | 0.015 |
| | Co-N | 2.14 | 1.0 | 1.00 | 3.02 | 0.0042 | |
| <i>R-1</i> -140°C | Co-O | 2.00 | 3.0 | 1.00 | -1.82 | 0.0075 | 0.0022 |
| | Co-N | 2.15 | 1.0 | 1.00 | 2.49 | 0.0054 | |
| <i>R-1</i> -180°C | Co-O | 1.98 | 3.0 | 1.00 | -2.10 | 0.0068 | 0.017 |
| | Co-N | 2.14 | 1.0 | 1.00 | 3.30 | 0.0045 | |
| <i>R-1</i> -re | Co-O | 2.08 | 5.0 | 1.00 | 0.39 | 0.0071 | 0.010 |
| | Co-N | 2.25 | 1.0 | 1.00 | 0.70 | 0.0050 | |

Table S6. Local structural fitting parameters of the Ni-O and Ni-N shells around Ni in *R-2*.

| Sample | Shell | R | N | S_0^2 | ΔE_0 | σ^2 | R-factor |
|----------------|-------|------|-----|---------|--------------|------------|----------|
| <i>R-2</i> | Ni-O | 2.05 | 5.0 | 1.00 | -1.03 | 0.0065 | 0.0048 |
| | Ni-N | 2.15 | 1.0 | 1.00 | 4.31 | 0.0032 | |
| <i>R-2</i> -de | Ni-O | 2.03 | 5.0 | 1.00 | -2.76 | 0.0080 | 0.0048 |
| | Ni-N | 2.16 | 1.0 | 1.00 | 4.80 | 0.0083 | |

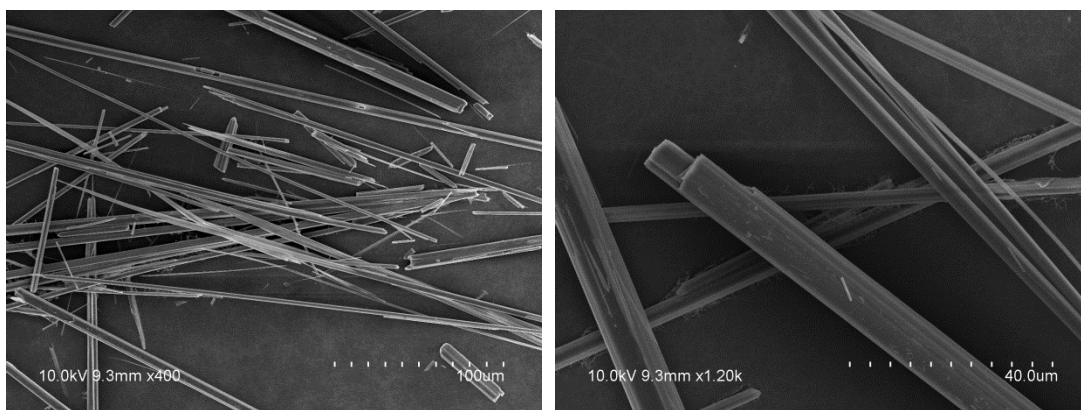


Figure S1. SEM images of compound *R-1*.

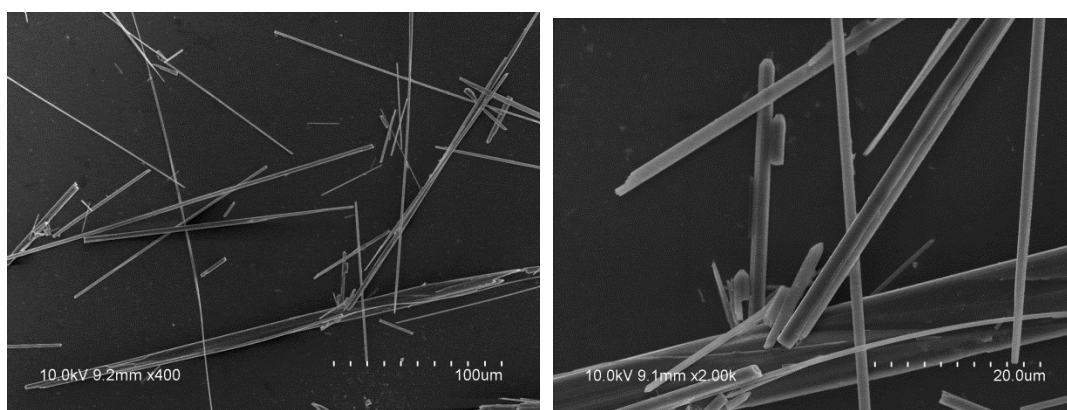


Figure S2. SEM images of compound *R-2*.

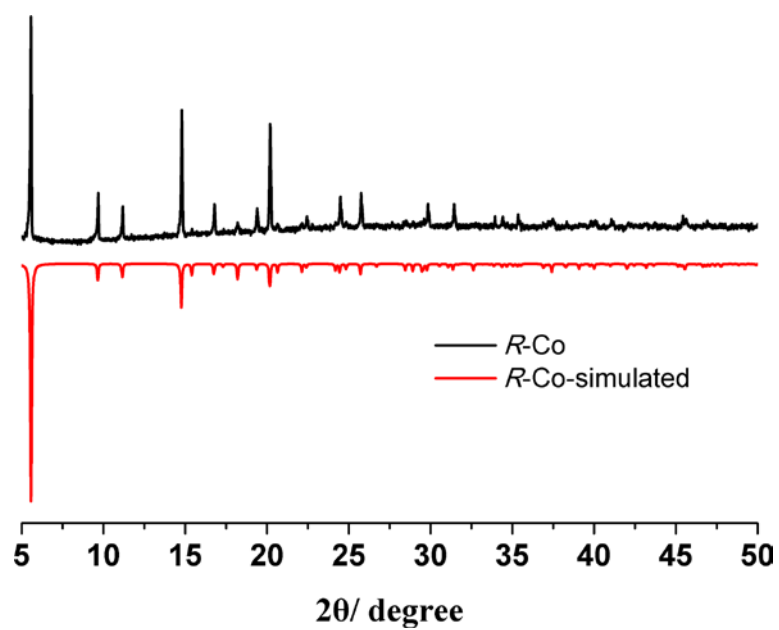


Figure S3. Powder XRD patterns for compound *R-1*.

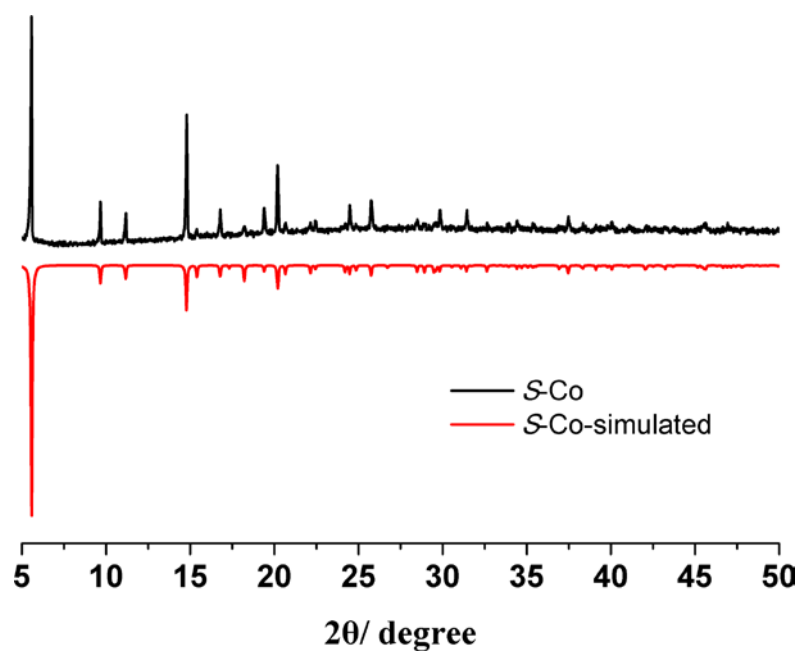


Figure S4. Powder XRD patterns for compound *S*-1.

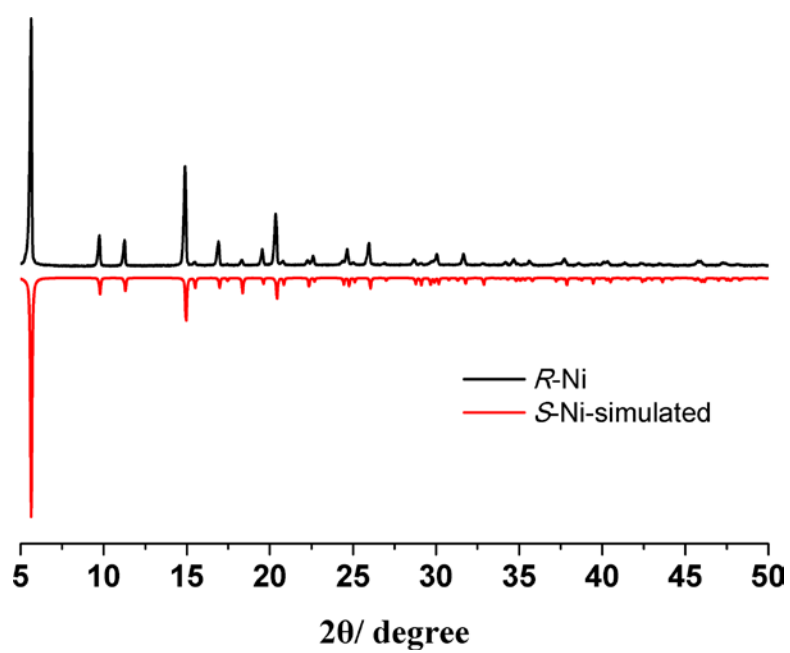


Figure S5. Powder XRD patterns for compound *R*-2.

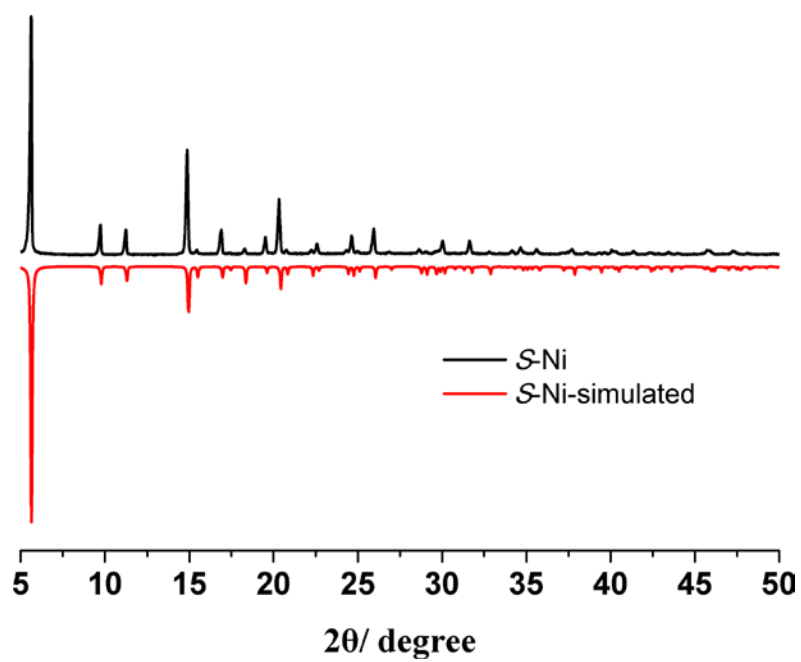


Figure S6. Powder XRD patterns for compound *S*-2.

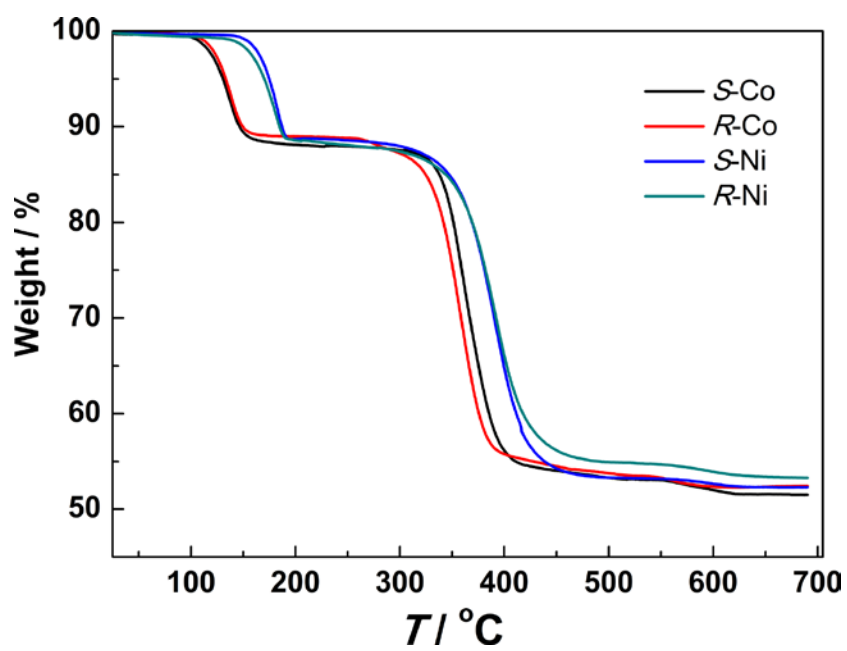


Figure S7. TGA curves for compounds *R*-1, *S*-1, *R*-2 and *S*-2.

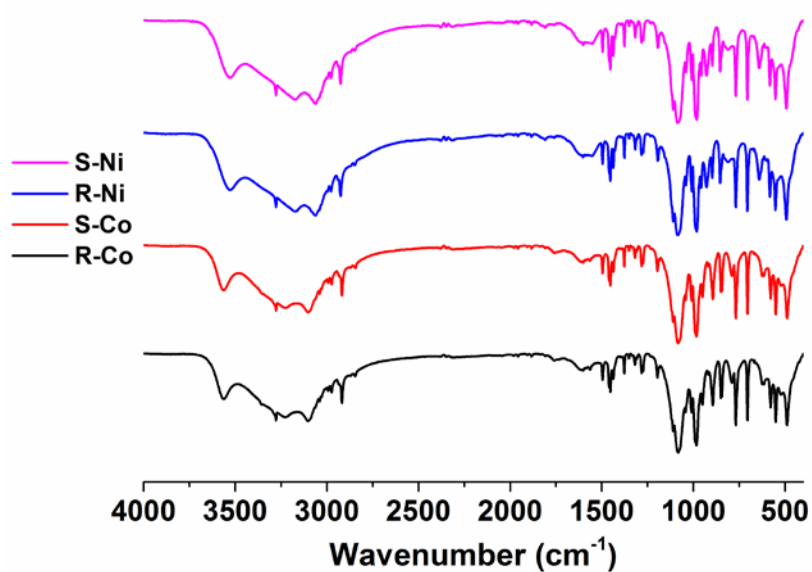


Figure S8. The IR spectra for compounds *R-1*, *S-1*, *R-2* and *S-2*.

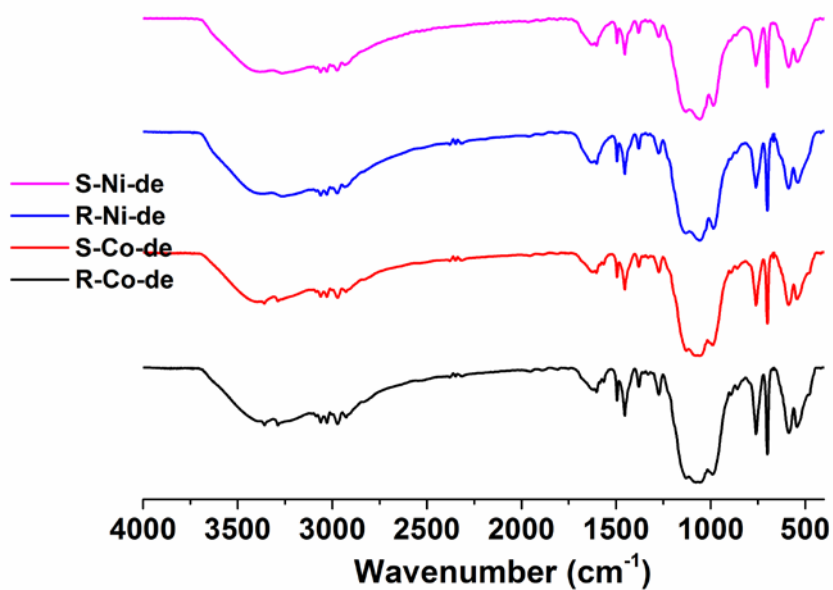


Figure S9. The IR spectra for compounds *R-1*, *S-1*, *R-2* and *S-2* after dehydration at 160°C (for **1**) and 180°C (for **2**) for 1 hour.

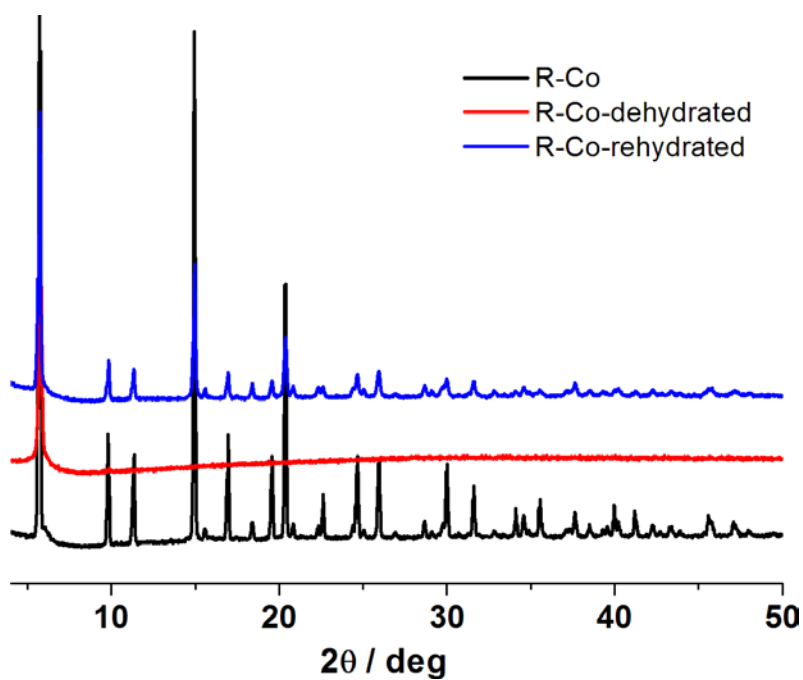


Figure S10. The powder XRD patterns for *R-1* before and after dehydration and re-hydration.

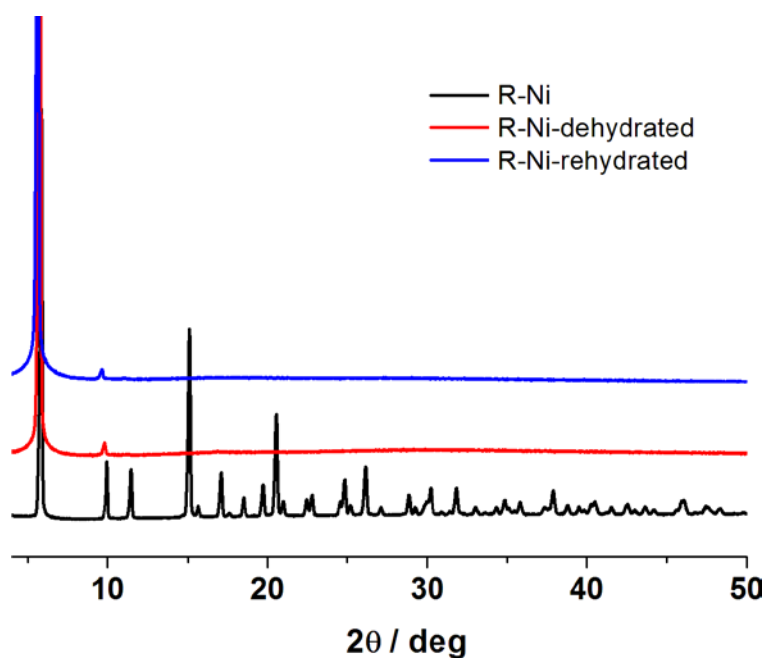


Figure S11. The powder XRD patterns for *R-2* before and after dehydration and re-hydration.

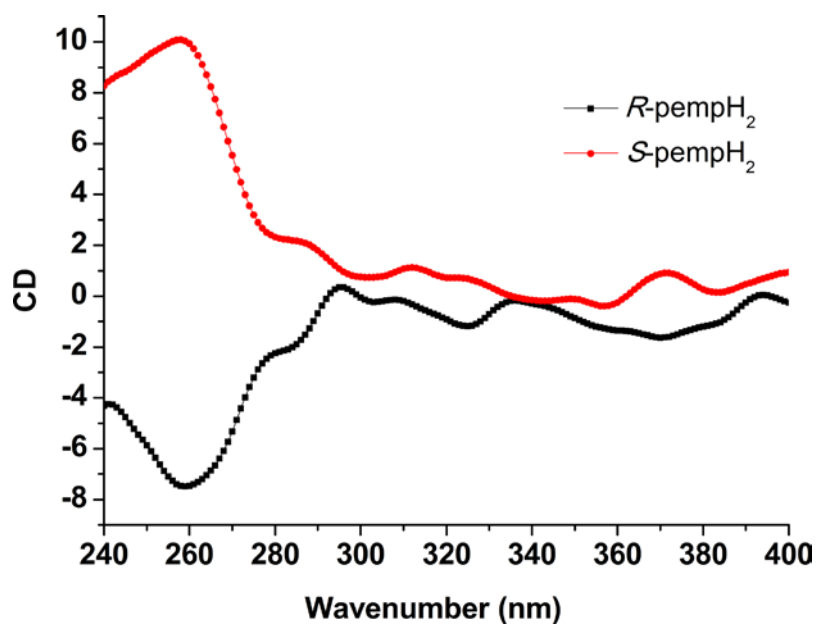


Figure S12. The CD spectra for *R*-pempH₂ (black) and *S*-pempH₂ (red) in the solid state.

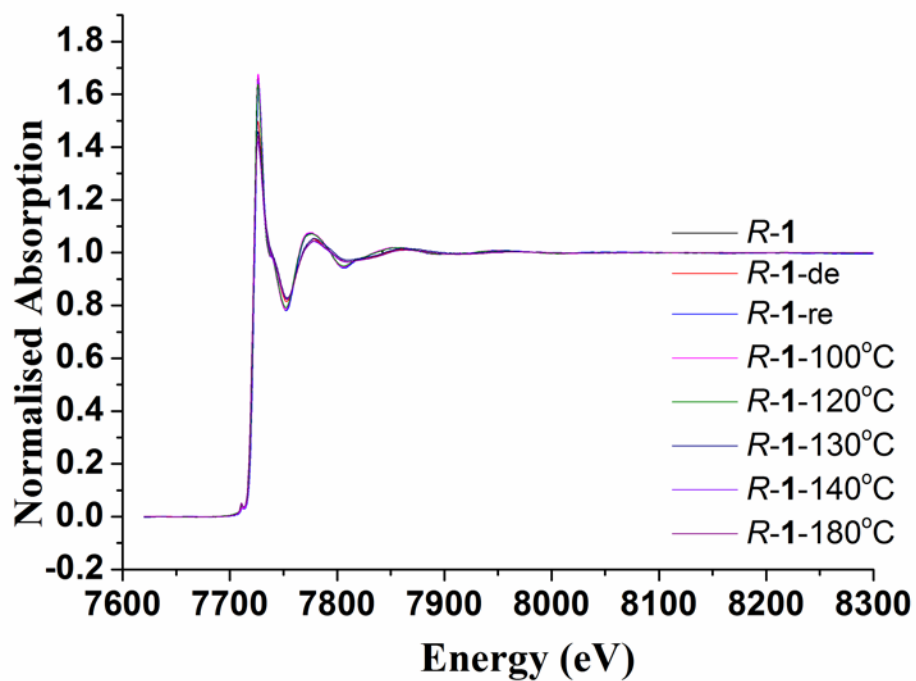


Figure S13. Co-K edge normalized EXAFS signals for *R*-1 and dehydrated samples.

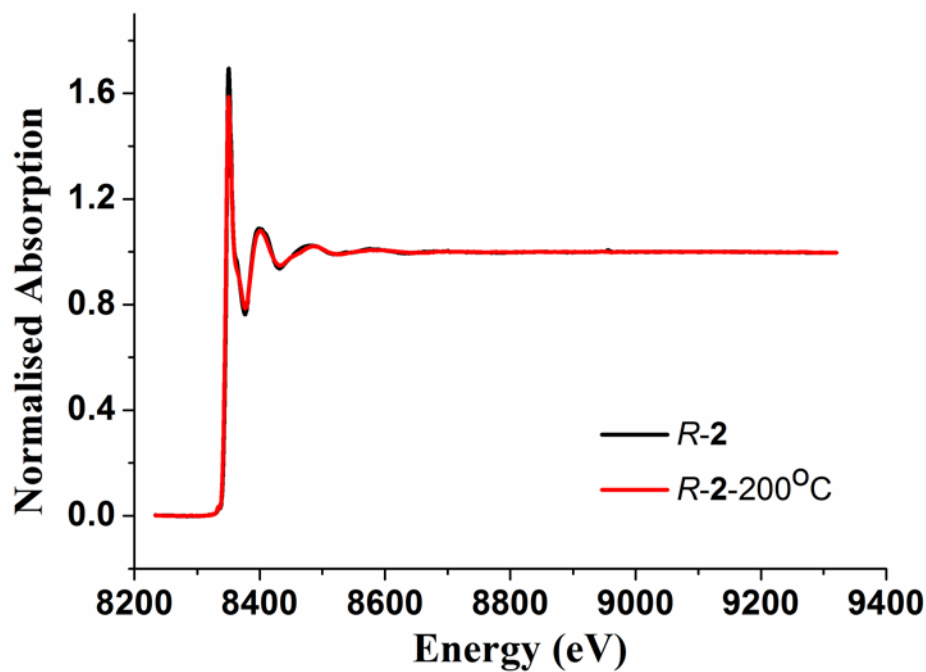


Figure S14. Ni-K edge normalized EXAFS signals for *R-2* and fully dehydrated samples.

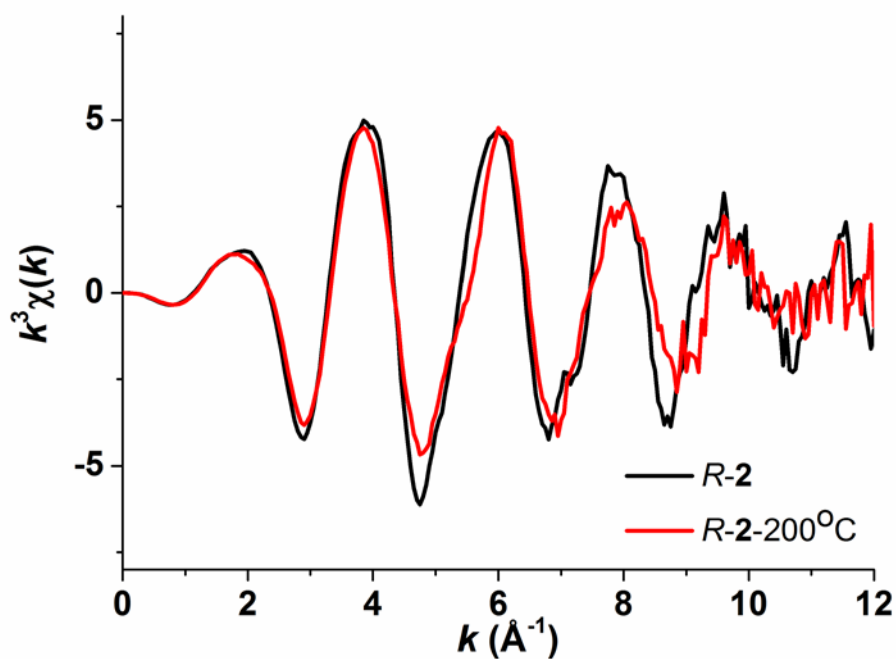


Figure S15. Ni-K edge k^3 -weight EXAFS signals taken at RT for the different dehydration temperature.

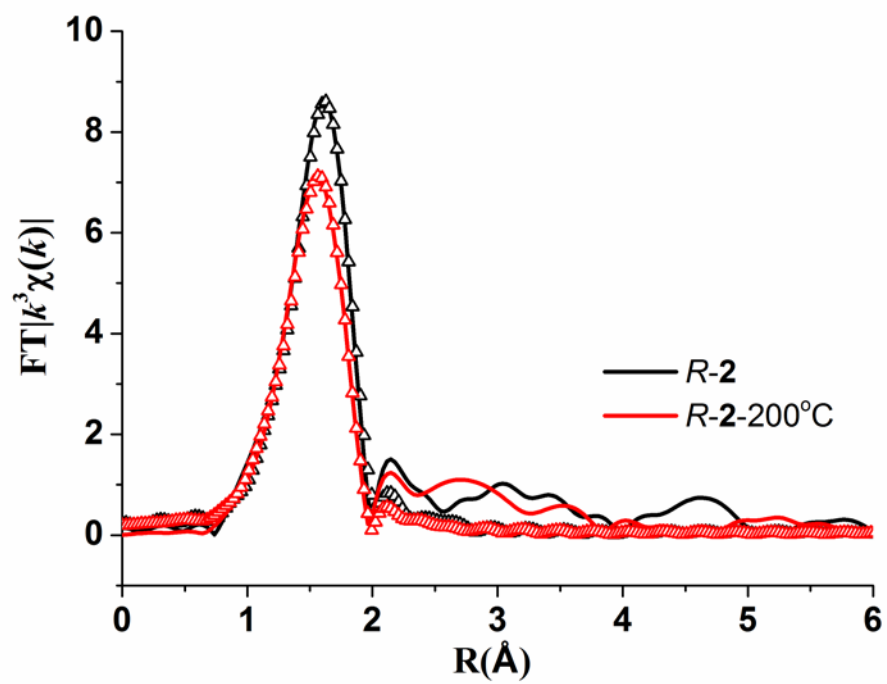


Figure S16. Fourier transformed space (R space) and their fitting curves (dotted lines) at Ni K-edge.

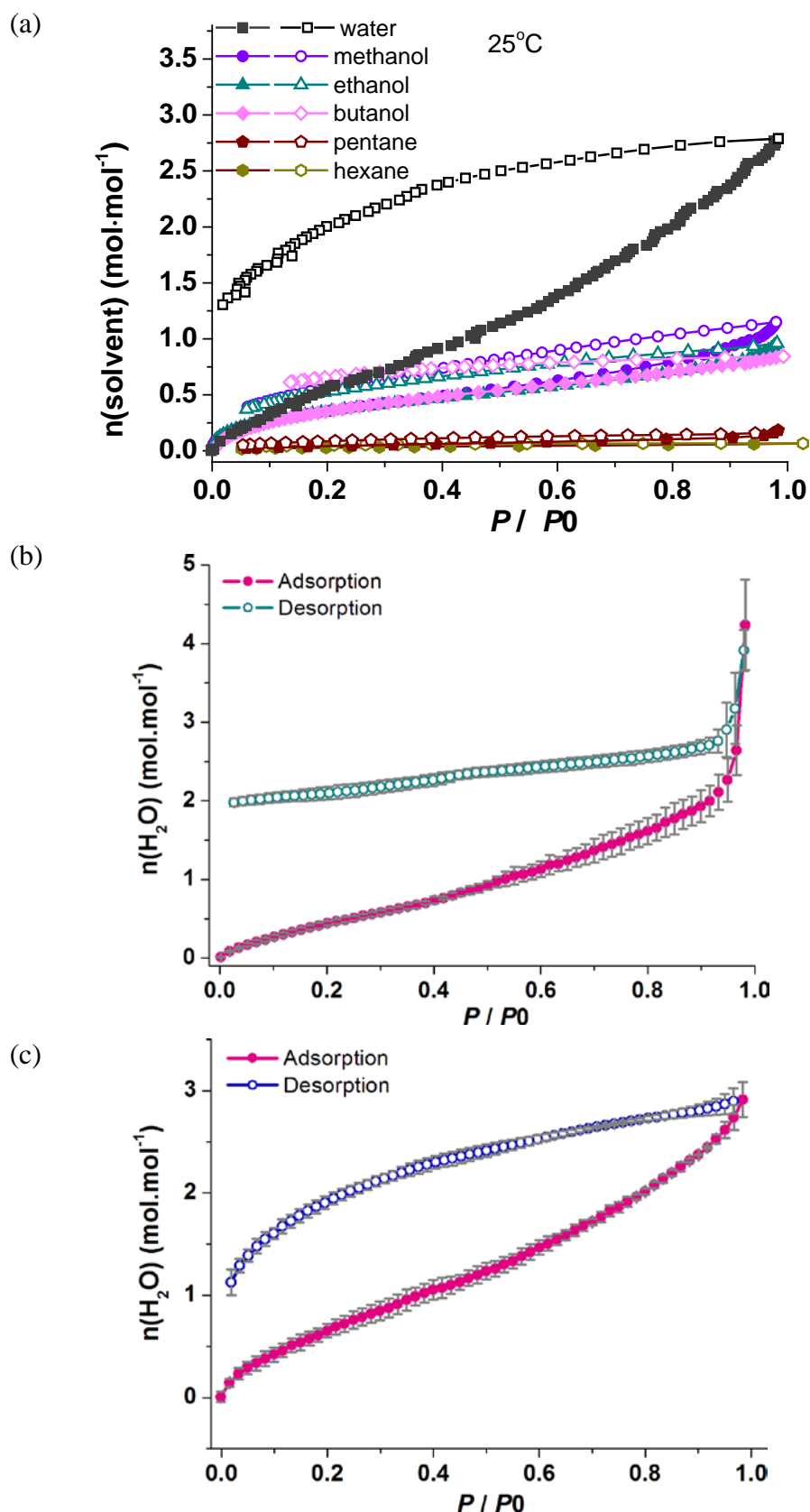


Figure S17. (a) Organic solvent adsorption (open circle) and desorption (filled circle) isotherms of **R-2** at 25 °C. Water isotherms of **R-1** (b) and **R-2** (c) at 25 °C showing error bars based on three repeating experiments.

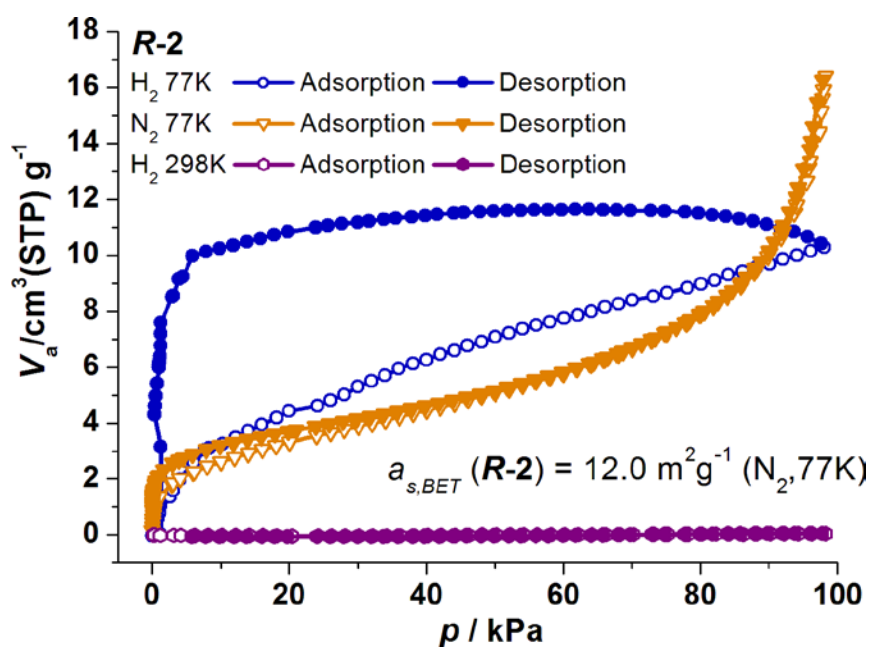
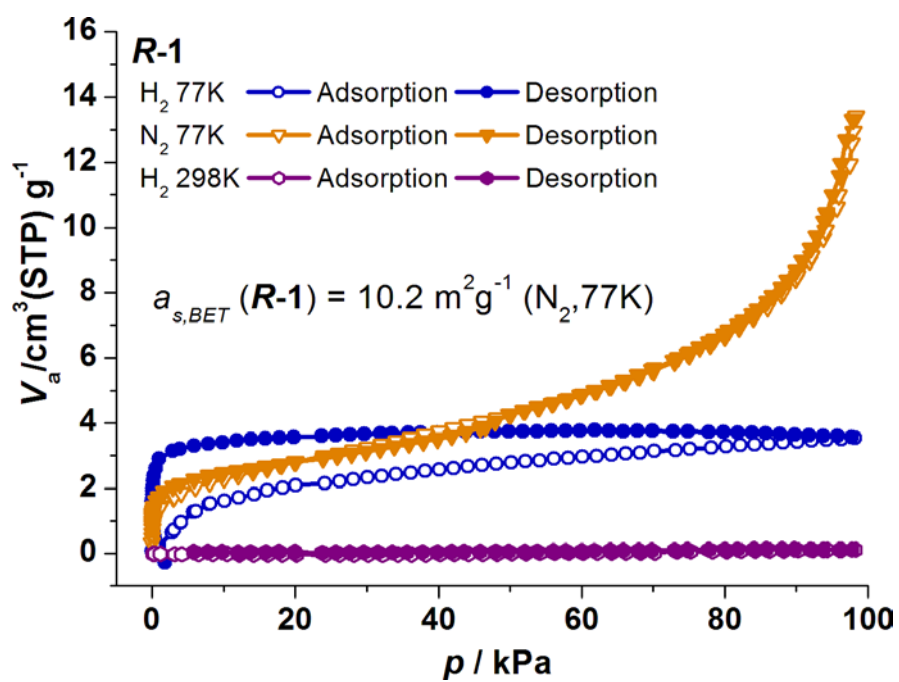


Figure S18. Nitrogen and hydrogen adsorption and desorption isotherms of **R-1** (top) and **R-2** (bottom) at -196°C (77 K).

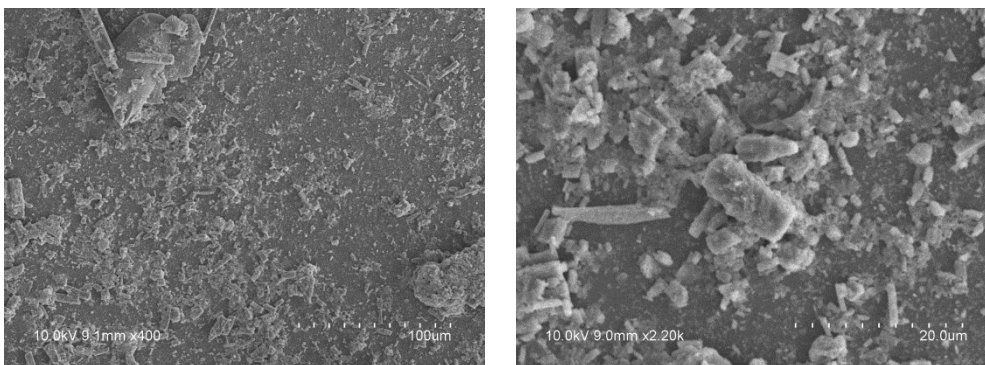


Figure S19. SEM images of sample *R-1* after grinding, which was used for proton conductivity measurements.

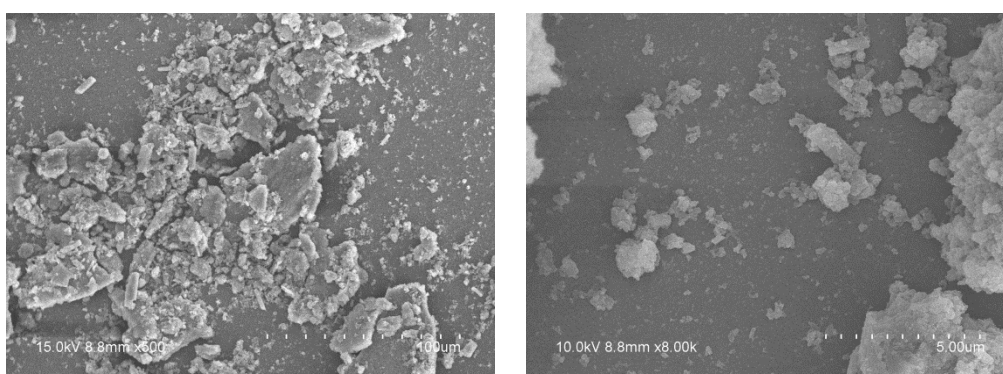


Figure S20. SEM images of sample *R-2* after grinding, which was used for proton conductivity measurements.

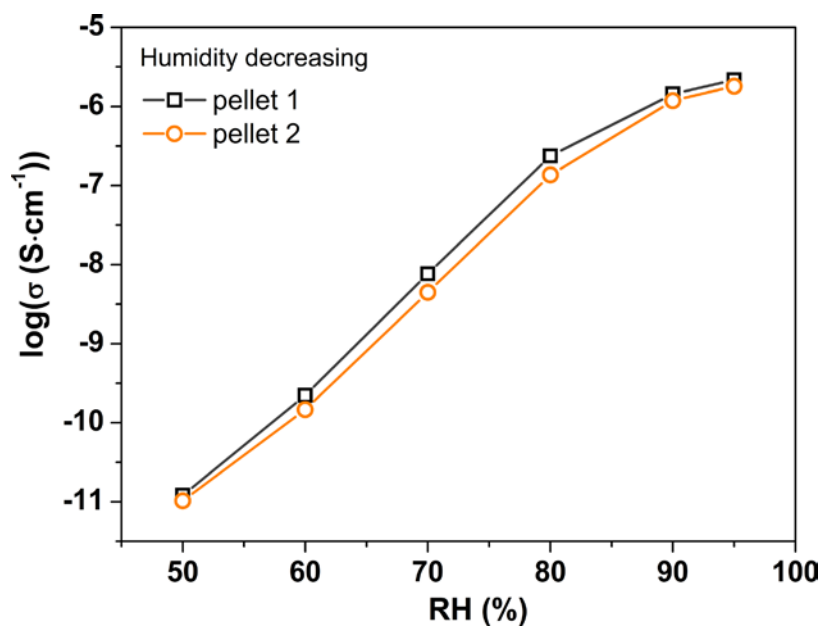


Figure S21. The plot of $\log(\sigma)$ vs. relative humidity for *R-1*. Two parallel experiments were performed using two pellets of the same compound.

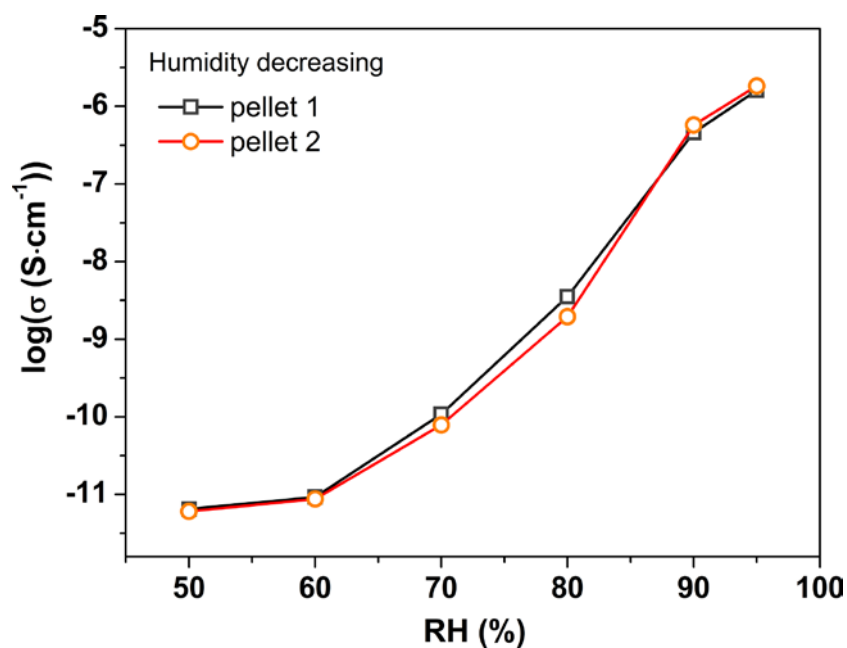


Figure S22. The plot of $\log(\sigma)$ vs. relative humidity for *R-2*. Two parallel experiments were performed using two pellets of the same compound.

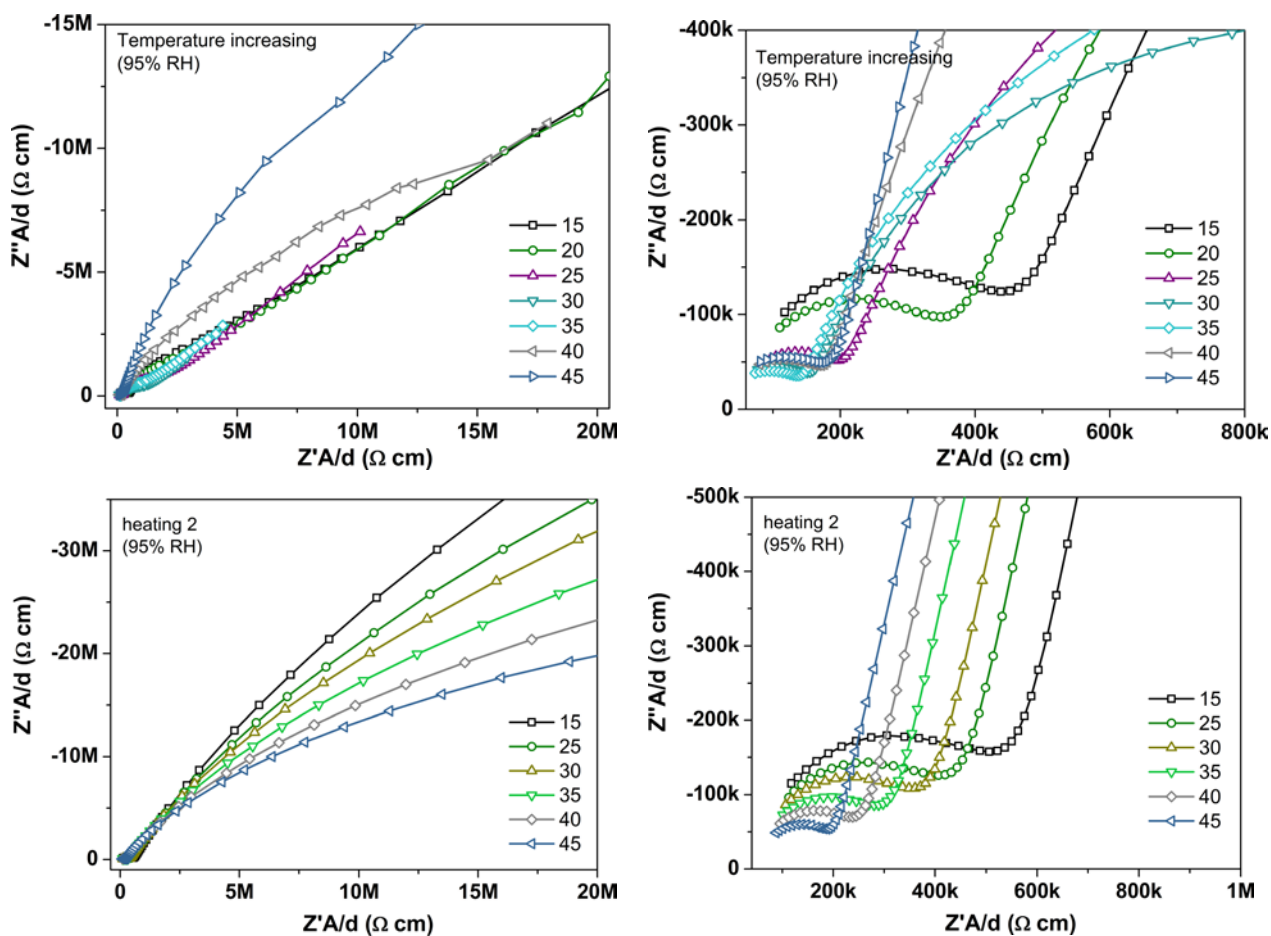


Figure S23. Nyquist plots of *R-1* measured from 15°C to 45°C at 95% RH during first (top) and second (bottom) circles of heating and cooling.

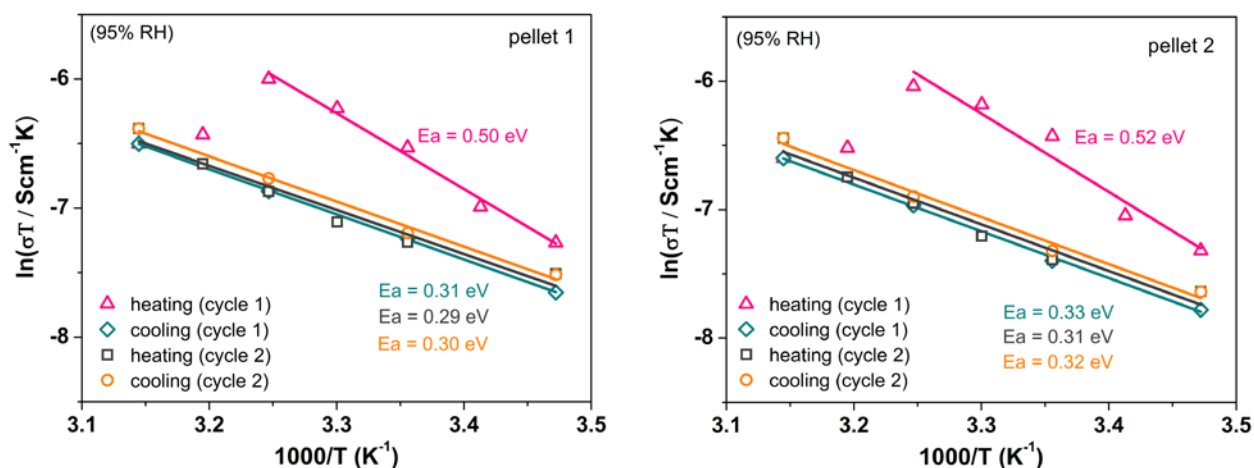


Figure S24. Arrhenius plots of the proton conductivity of R-1 measured at 95% RH. Two parallel experiments (left and right) were performed using two pellets of the same compound.

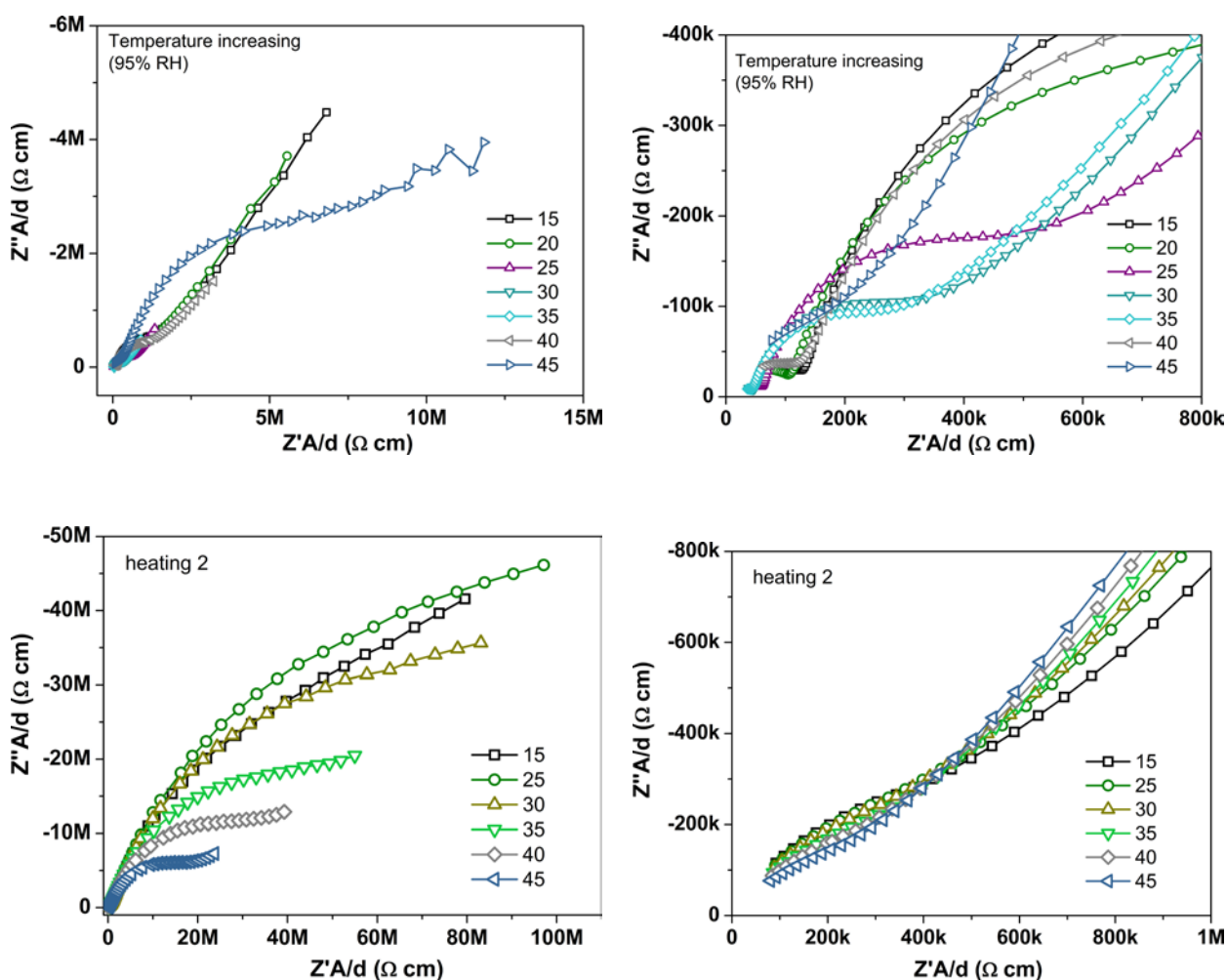


Figure S25. Nyquist plots of R-2 measured from 15°C to 45°C at 95% RH during first (top) and second (bottom) cycles of heating and cooling.

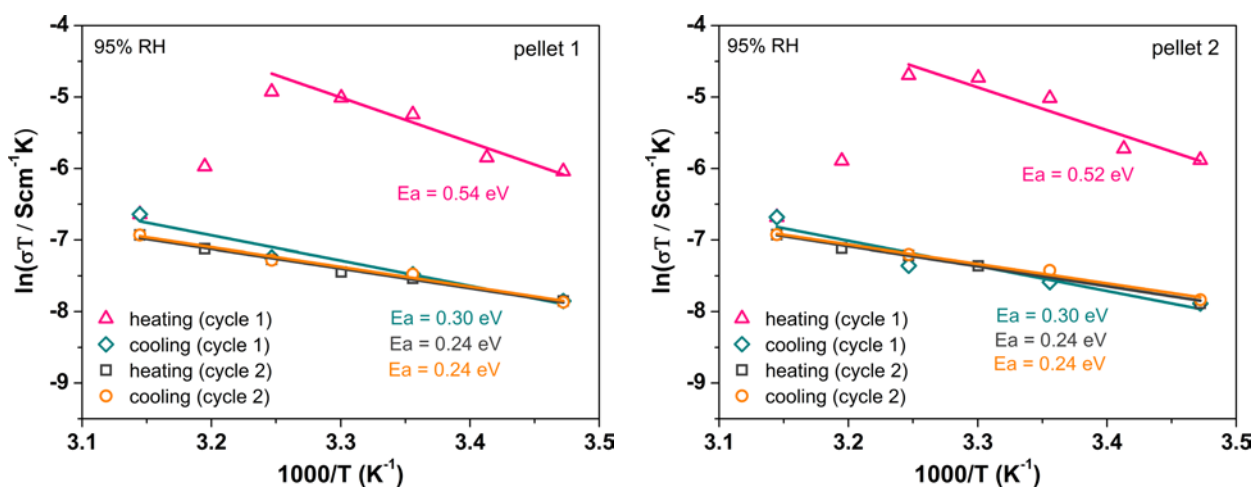


Figure S26. Arrhenius plots of the proton conductivity of *R-2* measured at 95% RH. Two parallel experiments (left and right) were performed using two pellets of the same compound.

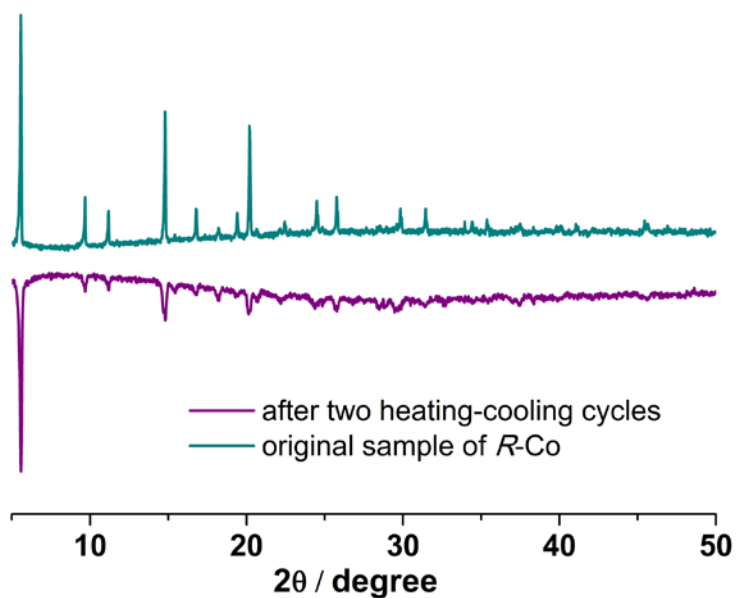


Figure S27. Powder XRD patterns for compound *R-1* before and after proton conductivity measurements.

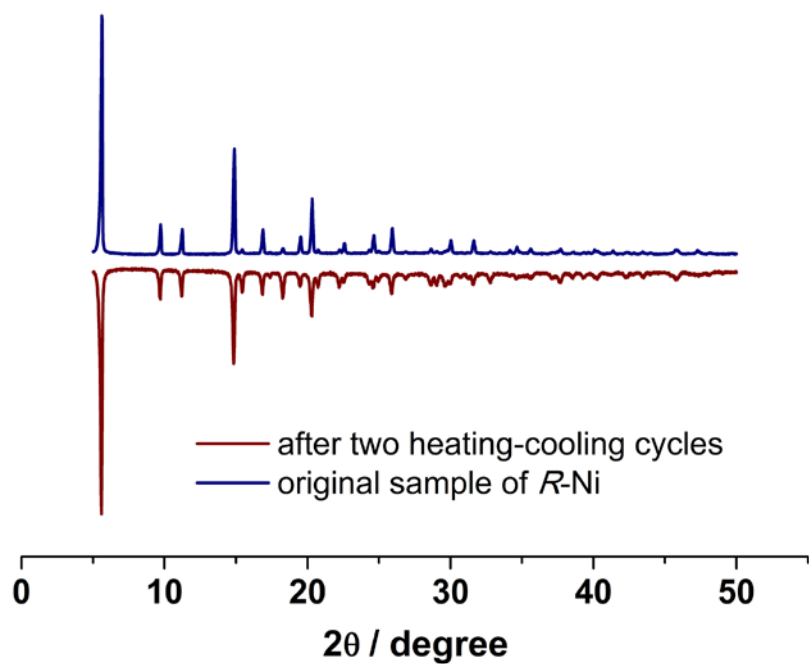


Figure S28. Powder XRD patterns for compound *R*-2 before and after proton conductivity measurements.

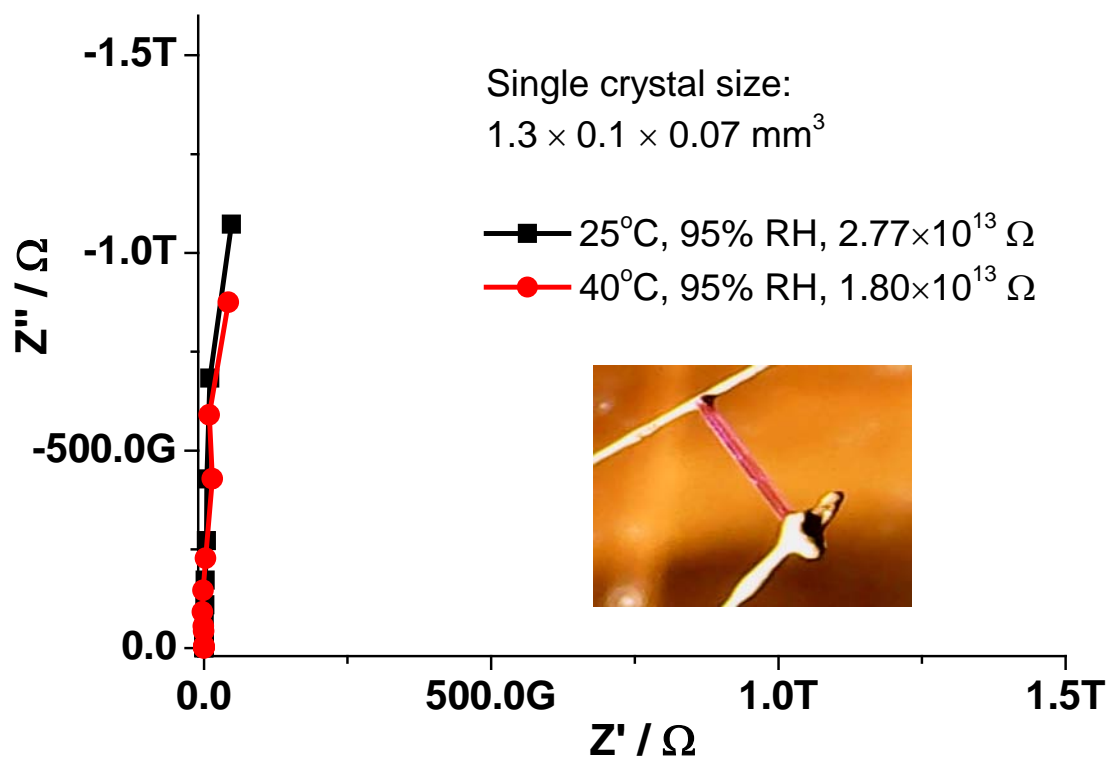


Figure S29. Nyquist plots of a single crystal of *R*-1 measured at 40 and 25°C (95% RH).